An innovative route to prepare in situ graded crosslinked PVA graphene electrospun mats for drug release

Emmanuel Fortunato Gulino, Maria Clara Citarrella, Andrea Maio, Roberto Scaffaro*

Department of Engineering, University of Palermo, Viale delle Scienze, ed. 6, 90128 Palermo, PA, Italy

*Corresponding author: roberto.scaffaro@unipa.it

Abstract

We present a fast, one step method to obtain PVA/graphene/chlorhexidine nanofibrous membranes, with a crosslinking gradient along their cross-section. Briefly, polymeric solutions were electrospun onto a heated plate, enabling the *in situ* crosslinking of PVA macromolecules. Of course, the crosslinking degree of such structures was found to decrease upon the distance from the plate during deposition. The outcomes reveal the crucial role of graphene, capable of promoting heat transfer throughout the entire structure, thus leading to 70-80% crosslinking degrees and preventing delamination issues. Such membranes were compared to untreated and oven thermally treated ones, and a robust relationship between processing, structure and properties was outlined, with a special focus on the release behaviour of such materials, which proved to be tuneable from instantaneous/burst to sustained release (up to 500 hours) by adjusting formulation and preparation technique.

Keywords: A. graphene; A. multifunctional composites; E. electrospinning; E. heat treatment.

1 Introduction

The development of drug delivery systems has been gaining increasing interest in the recent years, thanks to their ability to allow a sustained drug release at fixed rate for a definite time interval [1,2]. A drug delivery device able to release part of the drug at an initial therapeutic dose, followed by a slower and constant release could have many advantages including longer drug effectiveness, better balanced drug concentrations in the body and reduction of toxicity [3,4]. In order to obtain this kind of devices, the use of porous membranes represents a good strategy for a better control in drug release [3]. Electrospinning is a relatively facile method to fabricate polymeric nanofibrous and microfibrous membranes. Moreover, this technique, is increasingly used as an easy way to prepare several hybrid nanocomposites for wide use in filtration membranes, wound dressings, drug delivery systems and many others [5–25]. Electrospun fibers diameter depends on the rheological properties of the starting polymeric solution. In particular, an increase in solution viscosity allows obtaining fibers with larger diameter [26]. Moreover, post processing treatment, such as crosslinking, may induce an alteration of fibers diameter [27–35].

Poly (vinyl alcohol) (PVA) is a synthetic polymer, easily obtained through the polymerization of vinyl acetate followed by hydrolysis of the acetate groups. It is widely used for different applications in various fields, from food to medicine [36]. In recent times, PVA has attracted much attention in biomedical applications owing to its unique properties such as water solubility, promising biodegradability and excellent biocompatibility [36]. Among all the potential applications in this field, controlled drug release is one of the most widely studied [30,37–43]. Moreover, during electrospinning, PVA can form nanofibrous mats with good mechanical, biological and chemical properties. In addition, since PVA has plenty of hydroxyl groups, its mechanical properties and anti-solubility in water can be improved by either thermal or chemical crosslinking. In fact, this latter can dramatically modify the hydrophilicity of the membranes and, consequently, their solubility. Therefore, PVA membranes can be modified in order to obtain desirable drug release profiles by varying crosslinking degree. In the scientific literature, there are reported many methods to improve PVA mechanical properties including freeze-drying, heat treatments, irradiation, and chemical crosslinking [28–35,37,39,44–49]. In particular, crosslinking agents such as citric acid [29–32], glutaraldehyde [5,37,46–48] and sulfosuccinic acid [28,33], are commonly used for this purpose. Despite chemical crosslinking allows to easily achieving an excellent membrane stability [34] and tuning crosslinking degree by simply varying the amount of crosslinking agent added [30,46,48], in some case disadvantages including cost increase and potential toxic effects have been reported [44,49–52]. Hence, developing and optimizing a simple, one step, low-cost, non-toxic and green route for PVA crosslinking it is an important challenge.

Chlorhexidine (CHX) is an antibacterial agent active towards both gram-positive and gram-negative bacterial strains, as well as towards fungi in a dose-dependent manner, whose deactivation temperature is high enough to be melt-processed together with PVA and to be compatible with thermal crosslinking treatments.

The incorporation of nanosized reinforcements into a matrix is one of the most successful strategies to enhance the performance of biopolymers [53–60]. Moreover, it was demonstrated that the presence of nanoparticles in the matrix could tune drug release of those devices [61–64]. Among these, graphene nanoplatelets (GNP), belonging to the family of nanocarbons, are commonly used as fillers in polymer-based nanocomposites, aiming to enhance mechanical performance and to endow materials with electrical and thermal conductivity [65–67] and electromagnetic properties [68–70]. Therefore, the presence of GNP could enhance the effect of thermal crosslinking on the nanofibrous membranes, thus modifying drug release kinetics.

In order to obtain more versatile drug release kinetics, the development of multilayered structures with longitudinally solubility gradient could be an effective strategy. In particular, the more soluble layers

could provide quick drug release (e.g. useful for pain alleviation or bacterial growth prevention) while the less soluble ones could be suitable for ensuring long-term drug delivery. However, in some cases, the realization of this type of membranes requires the use of complex apparatuses and laborious and time consuming procedures [15,71–75]. Moreover, separation at the interface of adjacent layers can occur when the obtainment of multilayered structure is achieved by sequential electrospinning of multiple biomaterials with different properties [76,77]. Therefore, the development of an effective method to obtain a gradient water-soluble device would be a significant achievement in drug release device development.

Herein, we report a one step, green and facile route for improving the stability of PVA multi-layered membranes in aqueous environment, in order to obtain an efficient controlled released system. More in detail, a heated plate has been used as a collector of the electrospinning apparatus aiming to achieve progressive *in situ* crosslinking of PVA fibers. For sake of comparison, membranes were also prepared at 25 °C, and eventually subjected to post-processing thermal treatment in a vacuum oven, for achieving bulk crosslinking.

Ultimately, the aim of this work is to explore the possibility to tune the release of CHX, chosen as model compound, from PVA and PVA/GNP membranes by modifying their morpho-chemical features through different heat treatment techniques.

2 Experimental section

2.1 Materials and methods

Poly-vinyl-alcohol (PVA, Mw 89000-98000 Da, 99+% hydrolyzed) and chlorhexidine (CHX) in the form of diacetate salt (chemical formula: $C_{22}H_{30}Cl_2N_{10}\cdot(C_2H_4O_2)_2$, T_m=155 °C, water solubility = 19 g/L at 20 °C) were purchased from Sigma-Aldrich. Graphene nanoplatelets (GNP), trade name xGnP®, Grade C, were supplied by XG Sciences Inc., Lansing, MI, USA. Each particle consists in several sheets of graphene with an average thickness of approximately 10–20 nm, average width between 1 and 2 μm, and specific surface area of about 750 m^2/g. All the components were used as received. Four different types of formulation and three different routes were adopted to prepare twelve samples, whose codename, composition and preparation technique are listed in Table 1.

In all the cases, PVA (12 wt.%) was dissolved in deionized water at 95 °C under vigorous stirring for 4 h, whereas for preparing the (nano)composite mats, CHX and/or GNP were added to the polymeric solution respectively at 2 wt.% and 1 wt.% (relative to PVA).

Each polymeric solution was then poured into a 10 ml plastic syringe equipped with a 16-G metal needle and electrospun onto a grounded collector wrapped in an aluminium foil, by using a conventional

electrospinning equipment (Linari Engineering-Biomedical Division, Italy). The following operating conditions were kept constant for all the samples: feed rate = 3 ml/h, voltage applied = 20 kV, needle-to-collector distance=15 cm, electrospinning time= 2 hours. N-, O- and P-series membranes differ each other for some crucial parameters, as showed in Table 1. More in detail; N-series sample, taken as a reference, were obtained by electrospinning at T = 25 ± 3 °C; O-series samples were obtained from N-series ones via a post-processing thermal treatment, carried out in oven at 180 °C for 2 hours, with the purpose of attaining bulk crosslinking of fibrous mats; P-series sample, instead, were prepared by electrospinning the solutions onto a grounded collector heated at 180 °C, aiming to perform an *in situ* thermal treatment. Figure 1 provides a pictorial description of the three different routes adopted.

2.2 Characterization

Morphological analysis

The morphology of the nanofibers was observed by using a scanning electron microscope (Phenom ProX, Phenom-World, The Netherlands) with optical magnification range of 20–135x, electron magnification range of 80–130000x, maximal digital zoom of 12x, acceleration voltages of 15 kV. The microscope is equipped with a temperature controlled (25°C) sample holder. The samples were positioned on an aluminium stub using an adhesive carbon tape. Fiber diameter size distribution was measured using Image J software, equipped with Diameter J plugin [78]. More details can be found in our previous report [79].

Rheological characterization

Rheological properties of the polymeric solutions were analysed, using a rotational rheometer (ARES-G2) equipped with a 25-mm parallel-plate geometry. All tests were performed at 25 °C, in frequency sweep mode in the range 1-100 rad/s, by imposing constant stress of 1 Pa.

FT-IR/ATR analysis

The chemical and structural characterization of the samples were assessed by FT-IR/ATR analysis, carried out by using a Perkin-Elmer FT-IR/NIR Spectrum 400 spectrophotometer. The spectra were recorded in the wavenumber range 4000–400 cm^{-1}.

Mechanical properties

The mechanical behaviour of the membranes was investigated by tensile tests, carried out with a laboratory dynamometer (Instron model 3365, UK) equipped with a 1 kN load cell. The tests were performed on rectangular shaped specimens (10×90 mm) cut off from the membranes. The measurements

were performed by using a double crosshead speed: 1 mm min^{-1} for 2 min and 50 mm min^{-1} until fracture occurred. The grip distance was 20 mm, whereas the sample thickness was measured before each test. Seven specimens were tested for each sample and the outcomes of elastic modulus (E), tensile strength (TS), and elongation at break (EB), have been reported as average values ± standard deviations.

CHX release tests

A series of DI water solutions containing a known amount of CHX were analyzed by using UV/ vis spectrophotometer (model UVPC 2401, Shimadzu Italia s.r.l., Milan, Italy) in order to obtain a calibration line to correlate the absorbance band intensity of CHX and its concentration in DI water. The maximum absorbance band of CHX was detected at 230 nm. The release of the antiseptic from the membranes was investigated by immersing pre-weighed square specimens (10×10 mm^2 0.01g ca.) in 10 mL of DI water at 37 °C. The absorbance band intensity of the storage solutions was measured at specific time intervals and converted to CHX released through the calibration line. All the samples were immersed in 10 ml of fresh DI water after each measurement. Each measurement was performed in triplicate.

3 Results and discussion

Incorporating drugs and nanofillers may lead to an alteration of viscosity of the neat polymer solution [65]. This feature was investigated by performing the rheological analysis of the prepared solutions. Figure 2 shows rheological analysis of neat PVA, PVA/CHX, PVA/GNP and PVA/CHX-GNP solutions used for electrospinning. For all the solutions it was generally observed a pseudo plastic behavior, with all curves tending to Newtonian behavior in the low frequencies region, while showing remarkable shear thinning at higher frequencies, despite some differences from each other. In detail, the highest viscosity was exhibited by PVA/GNP solution, which showed the highest non-Newtonian properties, while PVA/CHX solution displayed the lowest viscosity and the largest extent of Newtonian region. In conclusion, viscosity follows the ascendant order: PVA/CHX < PVA/CHX-GNP < PVA < PVA/GNP.
It is known that rheological properties of starting polymeric solutions have a strong influence on the fibre diameter of resulting electrospun mats, which generally tends to increase upon increasing viscosity. Moreover, post processing treatments, such as crosslinking, may induce an alteration of fiber diameter [27–35]. Figure 3 shows cross-sectional SEM micrographs of non-treated, oven-treated and plate-treated PVA (a, a', a"), PVA/CHX (b, b', b"), PVA/GNP (c, c', c") and PVA/CHX-GNP (d, d', d") mats to provide an overview of the effect of different techniques and formulations on the morphology of the mats, whereas a more detailed morphological analysis, including cross-sectional and surface SEM micrographs, together with fiber size distribution is reported in Figure S1, S2 and S3, respectively for N-series, O-series and P-series mats (see Supporting Information). All N-series materials displayed a densely packed,

fibrous architecture, with approximately 50 μm thick cross-sections (Fig. 3 a-d). As regards surface morphology, each mat is constituted by randomly oriented continuous nanofibers with smooth surfaces and bead-free morphology (Figure S1 a'-d'), which display unimodal size distributions, whose maxima and mean values were found to differ each other. In detail, PVA_N fibers (Figure S1 a') showed an average diameter of 413 nm, whereas adding CHX or GNP respectively resulted in 25% thinner (Figure S1 b') or slightly thicker (6%) fibers (Figure S1 c'). Notably, in both cases the distributions proved to be narrower. Integrating both CHX and GNP (Figure S1 d') gave rise to mats having practically the same mean diameter as neat PVA, likely because the two opposite effects of additives had counterbalanced each other.

Noteworthy, the outcomes of morphological analysis are in full agreement with those of rheological characterization, thus pointing out that the variations detected in the average fiber diameters are governed by the solution viscosity [80].

With regard to oven-treated samples, such treatment clearly proved to affect the morphology of all membranes, when compared to the untreated ones. In detail, cross-sections of PVA_O (Figure 3 a'), PVA/CHX_O (Figure 3 b') PVA/GNP_O (Figure 3 c') and PVA/CHX-GNP_O (Figure 3 d') show a slightly increased thickness. This effect can be reasonably ascribed to the deformation of fibers induced by shrinkage during cross-linking, which led to the formation of wavy fibers, with ensuing section thickening [31]. By contrast, the average diameter of PVA_O fibers (Figure S2 a') and PVA/CHX_O (Figure S2 b') proved to decrease by 30 and 20 nm, respectively, if compared with their N-series counterparts. Indeed, thermal crosslinking treatment could also promote the coalescence of fibers, with ensuing increasing of diameter [48]. This effect is easily recognizable in PVA/GNP_O (Figure S2 c') in which the presence of GNP, due to its high thermal conductivity, likely leads to higher degree of crosslinking, thus enhancing the probability that two or more adjacent fibers coalesce. Likewise, in PVA/CHX-GNP_O (Figure S2 d') a plenty of coalesced fibers was observed. Hence, the presence of GNP generally leads to small reductions of fiber mean diameter. Moreover, morphological features proved to be unaltered along the entire cross-section of membranes, thus suggesting that oven treatment is capable of inducing a uniform bulk crosslinking.

It should be noted that in the case of plate-treatment, it is reasonable to assume that a thermal gradient might have established, with temperatures gradually decreasing as the layer-by-layer deposition on the hot plate proceeds. Consequently, such treatment is supposed to induce the formation of a graded/hierarchical crosslinked structure, as depicted in Figure 4, driven by the thermal gradient between plate layer (PL) and syringe one (SL). Therefore, the morphological analysis was performed onto the surface of both PL and SL (see subpanels a'-d' of Figure S3).

PVA_P (Figure 3 a'') and PVA/CHX_P (Figure 3 b'') membranes show an easily identifiable layered hierarchical structure. The layering of the membrane could be attributable to the different exposure temperatures of the various layers. In fact, it is known in the scientific literature that different temperatures induce different crosslinking degrees [81]. This effect leads to a different reduction in nanofibrous membranes solubility. Therefore, it could be assumed that PL shows a different solubility from SL, with this feature being likely responsible for the detachment between fibrous layers and thus for the formation of an evident stratified structure, as a function of time and temperature. As evidence of that, all the P-series mats are characterized by an increase in average diameter value in PL. In particular, PVA_P (Figure S3 a') and PVA/CHX_P (Figure S3 b') show a greater fibers' deformation and a higher degree of coalescence of fibers if compared with their counterparts thermally treated in oven. Therefore, the *in situ* crosslinking, on the plate layer, reasonably leads to a more intense crosslinking than that attainable in oven at the same conditions of temperature and time. The surface exposed to the syringe (SL), instead, shows practically the same average diameter as N-series membranes.

Since GNP thermal conductivity [65] facilitates heat conduction from PL to SL during the electrospinning process, it is possible to avoid (PVA/GNP_P, Figure 3 c'') or at least reduce (PVA/CHX-GNP_P, Figure 3 d'') delamination issues. Furthermore, PVA/GNP_P (Figure S3 c') showed average diameter values 25% higher than those of PVA/CHX-GNP_P in both sides (Figure S3 d'), reasonably because of the different viscosities of the two solutions.

The structural analysis of the materials prepared was evaluated by ATR-FTIR spectroscopy, as shown in Figure 5. In detail, such analysis was performed with the aim of confirming the successful crosslinking of PVA and the effective integration of CHX and GNP. In PVA-N (Figure 5 a-a'), the modes centered at 1000–1180 cm^{-1}, 2930 cm^{-1}, and 3000−3500 cm^{-1} were assigned to the C–O, $-CH_2-$ and –OH groups respectively [48]. Ether formation via condensation of -OH moieties can be therefore easily assessed by monitoring eventual changes in the spectral regions 3000-3500 cm^{-1} and 1000-1180 cm^{-1} When compared to N samples, all the thermally treated membranes, displayed the depletion of the intensity of –OH signal, owing to dehydroxylation and oxidation reactions between PVA hydroxyl groups during the stabilization process, thus testifying the effective crosslinking of the fibers [44]. Noteworthy, oven treated samples showed the strongest reduction of -OH intensity, followed by those treated *in situ* (P-series), whose intensities proved to be intermediate between those of oven crosslinked and N ones. Meanwhile, the analysis of C–O region (1800-1000 cm^{-1}) put into strong evidence that the contribution of peak centered at ca. 1150 cm^{-1}, ascribed to C-O-C ether bonding, become more prominent as the crosslinking degree increases. Hence, this spectral region was normalized to the intensity of C-O peak at 1098 cm^{-1} (see right panels) and the intensity ratio between the signals at 1150 cm^{-1} and 1098 cm^{-1} could provide further

evidence of the crosslinking events. Interestingly, PVA/GNP_N (Figure 5 c-c') and PVA/CHX-GNP_N (Figure 5 d-d') samples displayed a weak yet detectable peak at 1150 cm^{-1}, unlike the other untreated samples, thus suggesting that the presence of graphene might have promoted crosslinking phenomena even in the absence of thermal treatments.

Aiming to perform a quantitative analysis, crosslinking degree of the samples was calculated as the residual fraction after dissolution tests performed in deionized water at 37 °C for 5 hours. The outcomes, listed in Table 2, put into evidence some relevant aspects. First, among the N-series samples, those containing GNP displayed an unexpected crosslinking degree, as high as 25-30%, likely suggesting that such nanoparticles somehow acted as cross-linkers even in the absence of thermal treatments, in full agreement with what envisaged by spectroscopic analysis. Secondly, oven treatment effectively leads to fully crosslinked structures, as expected. The last consideration regards plate treatment, whose effectiveness proved to increase in the presence of GNP, reasonably due to their aforementioned high thermal conductivity. When compared to PVA_P and PVA/CHX_P, in fact, the materials containing a GNP amount as low as 1% resulted in crosslinking degrees 23% and 48% higher. These findings, in full agreement with all the other outcomes herein discussed, provide strong evidence about the robust formulation-processing-structure relationship of the systems investigated and points out the crucial role of GNP nanoparticles in promoting propagation of crosslinking pathways.

Type of formulation and processing technique, giving rise to materials with different and peculiar crosslinking degrees and structures, are supposed to affect the ultimate properties of the membranes. Therefore, the mechanical behavior of materials was investigated by tensile tests and the values of elastic modulus (E), tensile strength (TS) and elongation at break (EB) of the systems investigated are reported in Table 3. It was generally observed that adding CHX increased the membranes ductility, with obvious detrimental effects on E and TS. Indeed, this aspect could be easily ascribed to the plasticizing effect of the drug already envisaged by rheological tests. PVA/GNP_N displayed an opposite trend, with GNP nanoparticles imparting enhanced stiffness at the expense of ductility. Adding both GNP and CHX led to embrittlement of materials, thus being detrimental to breaking properties.

Regarding thermally treated membranes, an opposite behavior is observed between oven and plate series samples. The former ones, relying on the bulk propagation of crosslinking reactions, showed an expected increase of E and TS at the expense of EB [44,81]. Such behavior proved to be even more remarkable in GNP containing membranes, with this occurrence being reasonably ascribed to mechanical robustness of graphene, along with the increase of crosslinking degree due to the high thermal conductivity of graphene nanoparticles as already mentioned. P-series membranes, instead, show lower E and TS values if compared with N and O ones. This apparently surprising decrease could be likely attributed to their

morphology. In fact, as evidenced by SEM analysis, plate crosslinking promotes the formation of delaminated structure. It is important to highlight, once again, that the presence of graphene nanoparticles enhances the propagation of crosslinking events throughout the samples during heat treatment, thus reducing delamination phenomena. Therefore, *in situ* crosslinked GNP containing membranes (PVA/GNP_P and PVA/CHX-GNP_P) displayed mechanical performance higher than other P-series materials. Beyond this, it can be easily noted that in the presence of graphene, plate treatment endows the membranes with almost doubled breaking properties, if compared to oven treatment.

The release kinetics of CHX is shown in Figure 6 as the ratio M_t/M_∞ where M_t is the amount of drug released at time *t*, and M_∞ is the theoretical amount of CHX incorporated in the membranes. PVA/CHX_N and PVA/CHX-GNP_N release of CHX is characterized by a single step in which 100% of the drug molecules embedded in the nanofibers is released. For all crosslinked systems, CHX release is characterized by at least three phases: a burst release at the early stage of immersion time, a second phase characterized by the progressive depletion of CHX with ensuing slower release rate, and a final plateauing observed after long term immersion. In detail, PVA/CHX_O and PVA/CHX-GNP_O release about 50% of CHX in the first 5 h and reach the plateau region after about 500 h. This testifies that, effectively, oven crosslinked membranes are able to significantly slow down the release of CHX compared to N systems. The presence of GNP in PVA/CHX-GNP_O, promoting a more effective heat transfer and, therefore, higher crosslinking extent, also results in a further mitigation of burst release. Plate crosslinked systems show a more remarkable burst delivery, with about 70% of CHX released in the first 5 hours. This phenomenon can be reasonably attributed to a lower crosslinking degree in SL. However, the presence of GNP in PVA/CHX-GNP_P slows down the release in the burst phase, if compared to PVA/CHX_P one. This effect, once again, can be explained by considering the higher and more uniform crosslinking extent of such materials, which exhibited crosslinked fibers even in SL.

Such data were then fitted by using Peppas-Korsmeyer model, which enables the investigation of release kinetics through the following power law:

$$\frac{m_t}{m_\infty} = kt^n$$

Where n and k indicate, respectively, the diffusion exponent and the rate constant. According to this model, logarithmic plots of the CHX fraction released as a function of time were constructed and results are reported in Figure 7. It is worth noting that such model is valid only in the first portion of the curves (see blue-colored area in the plots of Figure 7). The slope (*n*) of fitting lines in this region provides

information about the release mechanism. In fact, when *n* is approximately 0.5, the drug delivery is driven by diffusive phenomena, whereas *n*=1 indicates that release mechanism is governed by swelling. *n* values between 0.5 and 1 indicate an anomalous release, governed by swelling and diffusive phenomena. In some cases, the presence of fillers or other additives capable of strongly interacting with drug or providing tortuous paths for molecule delivery, may hinder diffusion, thus giving n<0.5. Such burst region can be divided into two sub-regions, with the former one characterized by faster kinetics, likely due to the molecules of CHX available in the fibers' surface and thus readily delivered in aqueous medium, and the latter providing information about the actual capability of drug delivery device to establish a somehow controlled release. Noteworthy is the exceptional ability of crosslinked membranes, especially those containing graphene, in ensuring an almost Fickian release mechanism, unlike N ones, where CHX is immediately released because of the instantaneous dissolution of carrier. Indeed, logarithmic plots better allow evidencing the GNP role, which is of course more remarkable in plate systems than for oven ones, due to the improvement of heat transfer with positive repercussions on the propagation of crosslinking reactions throughout the entire membrane cross-section. In fact, oven-series materials, taking advantage of a bulk crosslinking, are quite able to provide controlled release, and the presence of GNP exerts a less remarkable effect.

Figure 8 and Figure 9 shows SEM images of surfaces and cross-sections of PVA/CHX_O, PVA/CHX_P and PVA/CHX-GNP_O, PVA/CHX-GNP_P, respectively, after immersion in distilled water at 37 °C for 0, 5 and 500 h. The images taken at 0 h, already shown previously in Figure 4 and Figure 5, are re-proposed to better highlight the time-dependent evolution of membranes' morphology during release. It can be noted that, depending on the type of treatment, remarkably different behaviour was observed. N-series membranes experienced a fast shrinkage, turning into transparent gel-like materials as soon as they are immersed in water.

Figure 8 a-f show SEM images of surfaces and sections of PVA/CHX_O after soaking in water for 0, 5 and 500h. After 5 hours in water, PVA/CHX_O show a quite stable structure, with a good retention of fiber morphology. After 500 h, although a slight alteration of the fibers is observed, the porosity of the membrane is still preserved. A different behaviour was observed for plate crosslinked membranes. PVA/CHX_P membrane (Figure 8 g-l), during the burst phase (5h), show a SL characterized by the coexistence of fibers and gels and a PL with negligible alterations of the fiber architecture, thus further confirming the higher extent of crosslinking attained in PL with respect to SL. After 500h, SL is totally transformed into a gel-like structure, while PL show a partial gel formation on the crosslinked fibers, likely attributable to the residual gel fraction of SL, once the remaining part came to complete dissolution.

This aspect seems to be confirmed by the dramatic thickness reduction observed in PVA/CHX_P after 500 h (see cross-sectional SEM micrograph in Figure 8 l).

PVA/CHX-GNP_O (Figure 9 a-f) maintains a stable structure with an almost unaltered morphology even after 500h of release in distilled water, owing to the aforementioned higher extent of crosslinked fibers. PVA/CHX-GNP_P (Figure 9 g-l), in the first 5h (i.e., burst stage), is characterized by a SL with a negligible gel formation (unlike the system containing only CHX in which a more intense gel formation is observed) and an unaltered PL. Notably, the thickness of the section (Figure 9 k) remains quite unaltered where it is possible to detect once again the poor gel formation of SL. After 500h, the SL is characterized by the coexistence of gel and fibers, while in PL the fibrous structure is preserved, in agreement with the analysis of cross-section (Figure 9 l) that shows a negligible reduction of thickness. Taken together, all these outcomes demonstrate that changing heat treatment process enables obtaining membranes with different, and tuneable, structures and properties.

4 Conclusions

A versatile, green and fast method to achieve PVA-based fibrous mats with graded crosslinking degree was presented and successfully applied to four types of formulation, comprising the eventual integration of graphene nanoplatelets (GNP) and/or chlorhexidine (CHX). Electrospinning polymeric aqueous solutions onto a heated plate allows constructing membranes whose crosslinking degree decreases along their cross-sections. It was elucidated the crucial role of GNP, capable of promoting the propagation of crosslinking events by virtue of its high thermal conductivity, thus preventing delamination issues in the graded membranes and increasing crosslinking degree, beyond the enhancement of mechanical performance. The results put into evidence that adjusting formulation enables tuning the crosslinking degree with ensuing differences in all the macroscopic properties, including mechanical robustness (up to +100% stiffness increments), and release behaviour. Graded membranes showed a multimodal drug delivery, with the scarcely crosslinked layers providing CHX release at the early stages of immersion, and highly crosslinked layers ensuring sustained release at constant rates after long-term immersion (up to 500 hours).

5 References

[1] Ratnaparkhi P, Jyoti GP, Mukesh. Sustained Release Oral Drug Delivery System -An Overview. International Journal of Pharma Research & Review IJPRR 2013;2:11–21.

[2] Jaimini M, Kothari AH. Sustained Release Matrix Type Drug Deliery System: a Review. Journal of Drug Delivery and Therapeutics 2012;2:142–8. https://doi.org/10.22270/jddt.v2i6.340.

[3] Berg MC, Zhai L, Cohen RE, Rubner MF. Controlled drug release from porous polyelectrolyte multilayers. Biomacromolecules 2006;7:357–64. https://doi.org/10.1021/bm050174e.

[4] Subramani M, Vekatashwaramoorthy N, Sambathkumar R. A Novel Approach on Role of Polymers Used In Sustained Release Drug Delivery System- A Review 2021;4929:170–8. https://doi.org/10.36348/sjmps.2021.v07i04.002.

[5] Wei X, Cai J, Lin S, Li F, Tian F. Colloids and Surfaces B : Biointerfaces Controlled release of monodisperse silver nanoparticles via in situ cross-linked polyvinyl alcohol as benign and antibacterial electrospun nanofibers. Colloids and Surfaces B: Biointerfaces 2021;197:111370. https://doi.org/10.1016/j.colsurfb.2020.111370.

[6] Article O. 17_Applied Microbiology and Biotechnology Efficacy of poly (lactic acid)/ carvacrol electrospun membranes against Staphylococcus aureus and Candida albicans in single and mixed cultures 2018:88–95.

[7] Wu J, Zhang Z, Gu J, Zhou W, Liang X, Zhou G, et al. Mechanism of a long-term controlled drug release system based on simple blended electrospun fibers. Journal of Controlled Release 2020;320:337–46. https://doi.org/10.1016/j.jconrel.2020.01.020.

[8] Dodero A, Alloisio M, Castellano M, Vicini S. Multilayer Alginate-Polycaprolactone Electrospun Membranes as Skin Wound Patches with Drug Delivery Abilities. ACS Applied Materials and Interfaces 2020;12:31162–71. https://doi.org/10.1021/acsami.0c07352.

[9] Zaidouny L, Abou-Daher M, Tehrani-Bagha AR, Ghali K, Ghaddar N. Electrospun nanofibrous polyvinylidene fluoride-co-hexafluoropropylene membranes for oil–water separation. Journal of Applied Polymer Science 2020;137:1–11. https://doi.org/10.1002/app.49394.

[10] Sun F, Huang SY, Ren HT, Li TT, Zhang Y, Lou CW, et al. Core-sheath structured TiO2@PVDF/PAN electrospun membranes for photocatalysis and oil-water separation. Polymer Composites 2020;41:1013–23. https://doi.org/10.1002/pc.25433.

[11] Augustine R, Rehman SRU, Ahmed R, Zahid AA, Sharifi M, Falahati M, et al. Electrospun chitosan membranes containing bioactive and therapeutic agents for enhanced wound healing. International Journal of Biological Macromolecules 2020;156:153–70. https://doi.org/10.1016/j.ijbiomac.2020.03.207.

[12] Bi H, Feng T, Li B, Han Y. In vitro and in vivo comparison study of electrospun PLA and PLA/PVA/SA fiber membranes for wound healing. Polymers 2020;12. https://doi.org/10.3390/POLYM12040839.

[13] Catania V, Lopresti F, Cappello S, Scaffaro R, Quatrini P. Innovative, ecofriendly biosorbent-biodegrading biofilms for bioremediation of oil-contaminated water. New Biotechnology 2020;58:25–31. https://doi.org/10.1016/j.nbt.2020.04.001.

[14] Ghafari R, Scaffaro R, Maio A, Gulino EF, lo Re G, Jonoobi M. Processing-structure-property relationships of electrospun PLA-PEO membranes reinforced with enzymatic cellulose nanofibers. Polymer Testing 2020;81:106182. https://doi.org/10.1016/j.polymertesting.2019.106182.

[15] Scaffaro R, Maio A, Gulino EF, Micale GDM. PLA-based functionally graded laminates for tunable controlled release of carvacrol obtained by combining electrospinning with solvent casting. Reactive and Functional Polymers 2020;148. https://doi.org/10.1016/j.reactfunctpolym.2020.104490.

[16] Elayappan V, Murugadoss V, Fei Z, Dyson PJ, Angaiah S. Influence of polypyrrole incorporated electrospun poly (vinylidene fluoride-co-hexafluoropropylene) nanofibrous composite membrane electrolyte on the photovoltaic performance of dye sensitized solar cell. Engineered Science 2020;10:78–84. https://doi.org/10.30919/es5e1007.

[17] Gao C, Deng W, Pan F, Feng X, Li Y. Superhydrophobic electrospun PVDF membranes with silanization and fluorosilanization co-functionalized CNTs for improved direct contact membrane distillation. Engineered Science 2020;9:35–43. https://doi.org/10.30919/es8d905.

[18] Panthi G, Ranjit R, Khadka S, Gyawali KR, Kim HY, Park M. Characterization and antibacterial activity of rice grain-shaped ZnS nanoparticles immobilized inside the polymer electrospun nanofibers. Advanced Composites and Hybrid Materials 2020;3:8–15. https://doi.org/10.1007/s42114-020-00141-9.

[19] Tsai P. Performance of masks and discussion of the inactivation of SARS-CoV-2. Engineered Science 2020;10:1–7. https://doi.org/10.30919/es8d1110.

[20] Deng L, Zhang H. Recent Advances in Probiotics Encapsulation by Electrospinning. ES Food & Agroforestry 2020:3–12. https://doi.org/10.30919/esfaf1120.

[21] Han G, Su Y, Feng Y, Lu N. Approaches for Increasing the β-phase Concentration of Electrospun Polyvinylidene Fluoride (PVDF) Nanofibers. ES Materials & Manufacturing 2019:75–80. https://doi.org/10.30919/esmm5f612.

[22] Panneerselvam P, Murugadoss V, Elayappan V, Lu N, Guo Z, Angaiah S. Influence of Anti-reflecting Nature of MgF2 Embedded Electrospun TiO2 Nanofibers Based Photoanode to Improve the Photoconversion Efficiency of DSSC. ES Energy & Environment 2018:99–105. https://doi.org/10.30919/esee8c153.

[23] Yang P, Zhao H, Yang Y, Zhao P, Zhao X, Yang L. Fabrication of N, P-Codoped Mo2C/Carbon Nanofibers Via Electrospinning as Electrocatalyst for Hydrogen Evolution Reaction. ES Materials & Manufacturing 2020:34–9. https://doi.org/10.30919/esmm5f618.

[24] Angaiah S, Murugadoss V, Arunachalam S, Panneerselvam P, Krishnan S. Influence of Various Ionic Liquids Embedded Electrospun Polymer Membrane Electrolytes on the Photovoltaic Performance of DSSC. Engineered Science 2018. https://doi.org/10.30919/es8d756.

[25] Xu G, Chen X, Zhu Z, Wu P, Wang H, Chen X, et al. Pulse gas-assisted multi-needle electrospinning of nanofibers 2020:98–113.

[26] Maio A, Gammino M, Gulino EF, Megna B, Fara P, Scaffaro R. Rapid One-Step Fabrication of Graphene Oxide-Decorated Polycaprolactone Three-Dimensional Templates for Water Treatment. ACS Applied Polymer Materials 2020. https://doi.org/10.1021/acsapm.0c00852.

[27] Enayati MS, Behzad T, Sajkiewicz P, Bagheri R, Ghasemi-Mobarakeh L, Łojkowski W, et al. Crystallinity study of electrospun poly (vinyl alcohol)

nanofibers: effect of electrospinning, filler incorporation, and heat treatment. Iranian Polymer Journal (English Edition) 2016;25:647–59. https://doi.org/10.1007/s13726-016-0455-3.

[28] Behavior T, Rynkowska E, Fatyeyeva K, Kujawa J. Chemically and Thermally Crosslinked PVA-Based Membranes : E ff ect on Swelling and 2019:7–9.

[29] Shi J, Yang E. Green electrospinning and crosslinking of polyvinyl alcohol/ citric acid. Journal of Nano Research 2015;32:32–42. https://doi.org/10.4028/www.scientific.net/JNanoR.32.32.

[30] Sabzi M, Afshari MJ, Babaahmadi M, Shafagh N. pH-dependent swelling and antibiotic release from citric acid crosslinked poly(vinyl alcohol) (PVA)/nano silver hydrogels. Colloids and Surfaces B: Biointerfaces 2020;188:110757. https://doi.org/10.1016/j.colsurfb.2019.110757.

[31] Stone SA, Gosavi P, Athauda TJ, Ozer RR. In situ citric acid crosslinking of alginate/polyvinyl alcohol electrospun nanofibers. Materials Letters 2013;112:32–5. https://doi.org/10.1016/j.matlet.2013.08.100.

[32] Nataraj D, Reddy R, Reddy N. Crosslinking electrospun poly (vinyl) alcohol fibers with citric acid to impart aqueous stability for medical applications. European Polymer Journal 2020;124:109484. https://doi.org/10.1016/j.eurpolymj.2020.109484.

[33] Rhim JW, Park HB, Lee CS, Jun JH, Kim DS, Lee YM. Crosslinked poly(vinyl alcohol) membranes containing sulfonic acid group: Proton and methanol transport through membranes. Journal of Membrane Science 2004;238:143–51. https://doi.org/10.1016/j.memsci.2004.03.030.

[34] Bolto B, Tran T, Hoang M, Xie Z. Crosslinked poly(vinyl alcohol) membranes. Progress in Polymer Science (Oxford) 2009;34:969–81. https://doi.org/10.1016/j.progpolymsci.2009.05.003.

[35] Kumar A, Ryparová P, Hosseinpourpia R, Adamopoulos S, Prošek Z, Žigon J, et al. Hydrophobicity and resistance against microorganisms of heat and chemically crosslinked poly(vinyl alcohol) nanofibrous membranes. Chemical Engineering Journal 2019;360:788–96. https://doi.org/10.1016/j.cej.2018.12.029.

[36] Kumar A, Han SS. PVA-based hydrogels for tissue engineering: A review. International Journal of Polymeric Materials and Polymeric Biomaterials 2017. https://doi.org/10.1080/00914037.2016.1190930.

[37] Nadem S, Ziyadi H, Hekmati M, Baghali M. Cross-linked poly(vinyl alcohol) nanofibers as drug carrier of clindamycin. Polymer Bulletin 2020. https://doi.org/10.1007/s00289-019-03027-z.

[38] Tampau A, González-Martínez C, Chiralt A. Polyvinyl alcohol-based materials encapsulating carvacrol obtained by solvent casting and electrospinning. Reactive and Functional Polymers 2020. https://doi.org/10.1016/j.reactfunctpolym.2020.104603.

[39] Singh B, Pal L. Sterculia crosslinked PVA and PVA-poly(AAm) hydrogel wound dressings for slow drug delivery: Mechanical, mucoadhesive, biocompatible and permeability properties. Journal of the Mechanical Behavior of Biomedical Materials 2012;9:9–21. https://doi.org/10.1016/j.jmbbm.2012.01.021.

[40] Yang D, Li Y, Nie J. Preparation of gelatin/PVA nanofibers and their potential application in controlled release of drugs. Carbohydrate Polymers 2007;69:538–43. https://doi.org/10.1016/j.carbpol.2007.01.008.

[41] Song W, Yu X, Markel DC, Shi T, Ren W. Coaxial PCL/PVA electrospun nanofibers: Osseointegration enhancer and controlled drug release device. Biofabrication 2013;5. https://doi.org/10.1088/1758-5082/5/3/035006.

[42] Morita R, Honda R, Takahashi Y. Development of oral controlled release preparations, a PVA swelling controlled release system (SCRS). II. In vitro and in vivo evaluation. Journal of Controlled Release 2000;68:115–20. https://doi.org/10.1016/S0168-3659(00)00244-3.

[43] Morita R, Honda R, Takahashi Y. Development of oral controlled release preparations, a PVA swelling controlled release system (SCRS). I. Design of SCRS and its release controlling factor. Journal of Controlled Release 2000;63:297–304. https://doi.org/10.1016/S0168-3659(99)00203-5.

[44] Zhu J, Lv S, Yang T, Huang T, Yu H, Zhang Q, et al. Facile and Green Strategy for Designing Ultralight, Flexible, and Multifunctional PVA Nanofiber-Based Aerogels. Advanced Sustainable Systems 2020. https://doi.org/10.1002/adsu.201900141.

[45] Zhan F, Yan X, Li J, Sheng F, Li B. Encapsulation of tangeretin in PVA/PAA crosslinking electrospun fibers by emulsion-electrospinning: Morphology characterization, slow-release, and antioxidant activity assessment. Food Chemistry 2021. https://doi.org/10.1016/j.foodchem.2020.127763.

[46] Destaye AG, Lin CK, Lee CK. Glutaraldehyde vapor cross-linked nanofibrous PVA mat with in situ formed silver nanoparticles. ACS Applied Materials and Interfaces 2013;5:4745–52. https://doi.org/10.1021/am401730x.

[47] Moreno-Cortez IE, Romero-García J, González-González V, García-Gutierrez DI, Garza-Navarro MA, Cruz-Silva R. Encapsulation and immobilization of papain in electrospun nanofibrous membranes of PVA cross-linked with glutaraldehyde vapor. Materials Science and Engineering C 2015;52:306–14. https://doi.org/10.1016/j.msec.2015.03.049.

[48] Wei X, Cai J, Lin S, Li F, Tian F. Controlled release of monodisperse silver nanoparticles via in situ cross-linked polyvinyl alcohol as benign and antibacterial electrospun nanofibers. Colloids and Surfaces B: Biointerfaces 2021;197:111370. https://doi.org/10.1016/j.colsurfb.2020.111370.

[49] Ma CB, Du B, Wang E. Self-Crosslink Method for a Straightforward Synthesis of Poly(Vinyl Alcohol)-Based Aerogel Assisted by Carbon Nanotube. Advanced Functional Materials 2017;27:1–8. https://doi.org/10.1002/adfm.201604423.

[50] Chen HB, Hollinger E, Wang YZ, Schiraldi DA. Facile fabrication of poly(vinyl alcohol) gels and derivative aerogels. Polymer 2014;55:380–4. https://doi.org/10.1016/j.polymer.2013.07.078.

[51] Javadi A, Zheng Q, Payen F, Javadi A, Altin Y, Cai Z, et al. Polyvinyl alcohol-cellulose nanofibrils-graphene oxide hybrid organic aerogels. ACS Applied Materials and Interfaces 2013;5:5969–75. https://doi.org/10.1021/am400171y.

[52] Chen HB, Liu B, Huang W, Wang JS, Zeng G, Wu WH, et al. Fabrication and properties of irradiation-cross-linked poly(vinyl alcohol)/clay aerogel composites. ACS Applied Materials and Interfaces 2014;6:16227–36. https://doi.org/10.1021/am504418w.

[53] DeLeon VH, Nguyen TD, Nar M, D'Souza NA, Golden TD. Polymer nanocomposites for improved drug delivery efficiency. Materials Chemistry and Physics 2012;132:409–15. https://doi.org/10.1016/j.matchemphys.2011.11.046.

[54] Armentano I, Dottori M, Fortunati E, Mattioli S, Kenny JM. Biodegradable polymer matrix nanocomposites for tissue engineering: A

review. Polymer Degradation and Stability 2010;95:2126–46. https://doi.org/10.1016/j.polymdegradstab.2010.06.007.

[55] Yu Z, Bai Y, Wang JH, Li Y. Effects of Functional Additives on Structure and Properties of Polycarbonate-Based Composites Filled with Hybrid Chopped Carbon Fiber/Graphene Nanoplatelet Fillers. ES Energy & Environment 2021:66–76. https://doi.org/10.30919/esee8c434.

[56] Sun J, Zhang X, Du Q, Murugadoss V, Wu D, Guo Z. The Contribution of Conductive Network Conversion in Thermal Conductivity Enhancement of Polymer Composite: A Theoretical and Experimental Study. ES Materials & Manufacturing 2021:53–65. https://doi.org/10.30919/esmm5f450.

[57] Zhou Y, Wang P, Ruan G, Xu P, Ding Y. Synergistic Effect of P[MPEGMA-IL] Modified Graphene on Morphology and Dielectric Properties of PLA/PCL Blends. ES Materials & Manufacturing 2020:20–9. https://doi.org/10.30919/esmm5f928.

[58] Yuan B, Li L, Murugadoss V, Vupputuri S, Wang J, Alikhani N, et al. Nanocellulose-based composite materials for wastewater treatment and waste-oil remediation. ES Food & Agroforestry 2020:41–52. https://doi.org/10.30919/esfaf0004.

[59] Zhou Y, Wu S, Ma Y, Zhang H, Zeng X, Wu F, et al. Recent Advances in Organic/Composite Phase Change Materials for Energy Storage. ES Energy & Environment 2020;c:28–40. https://doi.org/10.30919/esee8c150.

[60] Huang J, Luo Y, Weng M, Yu J, Sun L, Zeng H, et al. Advances and Applications of Phase Change Materials (PCMs) and PCMs-based Technologies. ES Materials & Manufacturing 2021:23–39. https://doi.org/10.30919/esmm5f458.

[61] Scaffaro R, Botta L, Maio A, Gallo G. PLA graphene nanoplatelets nanocomposites: Physical properties and release kinetics of an antimicrobial agent. Composites Part B: Engineering 2017;109:138–46. https://doi.org/10.1016/j.compositesb.2016.10.058.

[62] Scaffaro R, Botta L, Maio A, Mistretta MC, la Mantia FP. Effect of graphene nanoplatelets on the physical and antimicrobial properties of biopolymer-based nanocomposites. Materials 2016;9. https://doi.org/10.3390/ma9050351.

[63] de Jong WH, Borm PJA. Drug delivery and nanoparticles: Applications and hazards. International Journal of Nanomedicine 2008;3:133–49. https://doi.org/10.2147/ijn.s596.

[64] Hu H, Liu H, Zhang D, Wang J, Qin G, Zhang X. pH and electromagnetic dual-remoted drug delivery based on bimodal superparamagnetic Fe3O4@Porous silica nanoparticles. Engineered Science 2018;2:43–8. https://doi.org/10.30919/es8d136.

[65] Scaffaro R, Maio A, Botta L, Gulino EF, Gulli D. Tunable release of Chlorhexidine from Polycaprolactone-based filaments containing graphene nanoplatelets. European Polymer Journal 2019;110:221–32. https://doi.org/10.1016/j.eurpolymj.2018.11.031.

[66] Li Y, Porwal H, Huang Z, Zhang H, Bilotti E, Peijs T. Enhanced Thermal and Electrical Properties of Polystyrene-Graphene Nanofibers via Electrospinning. Journal of Nanomaterials 2016;2016. https://doi.org/10.1155/2016/4624976.

[67] Kaur T, Thirugnanam A, Pramanik K. Effect of carboxylated graphene nanoplatelets on mechanical and in-vitro biological properties of polyvinyl alcohol nanocomposite scaffolds for bone tissue engineering. Materials Today Communications 2017;12:34–42. https://doi.org/10.1016/j.mtcomm.2017.06.004.

[68] Lu X, Zhu D, Li X, Li M, Chen Q, Qing Y. Gelatin-derived N-doped hybrid carbon nanospheres with an adjustable porous structure for enhanced electromagnetic wave absorption. Advanced Composites and Hybrid Materials 2021. https://doi.org/10.1007/s42114-021-00258-5.

[69] Wu N, Qiao J, Liu J, Du W, Xu D, Liu W. Strengthened electromagnetic absorption performance derived from synergistic effect of carbon nanotube hybrid with Co@C beads. Advanced Composites and Hybrid Materials 2018;1:149–59. https://doi.org/10.1007/s42114-017-0008-z.

[70] Xie P, Liu Y, Feng M, Niu M, Liu C, Wu N, et al. Hierarchically porous Co/C nanocomposites for ultralight high-performance microwave absorption. Advanced Composites and Hybrid Materials 2021. https://doi.org/10.1007/s42114-020-00202-z.

[71] Grey CP, Newton ST, Bowlin GL, Haas TW, Simpson DG. Gradient fiber electrospinning of layered scaffolds using controlled transitions in fiber diameter. Biomaterials 2013;34:4993–5006. https://doi.org/10.1016/j.biomaterials.2013.03.033.

[72] Jin G, Shin M, Kim SH, Lee H, Jang JH. SpONGE: Spontaneous organization of numerous-layer generation by electrospray. Angewandte Chemie - International Edition 2015;54:7587–91. https://doi.org/10.1002/anie.201502177.

[73] Zonderland J, Rezzola S, Wieringa P, Moroni L. Fiber diameter, porosity and functional group gradients in electrospun scaffolds. Biomedical Materials (Bristol) 2020;15. https://doi.org/10.1088/1748-605X/ab7b3c.

[74] Balakrishnan M, Shrestha P, Ge N, Lee C, Fahy KF, Zeis R, et al. Designing Tailored Gas Diffusion Layers with Pore Size Gradients via Electrospinning for Polymer Electrolyte Membrane Fuel Cells. ACS Applied Energy Materials 2020;3:2695–707. https://doi.org/10.1021/acsaem.9b02371.

[75] Wulkersdorfer B, Kao KK, Agopian VG, Ahn A, Dunn JC, Wu BM, et al. Bimodal porous scaffolds by sequential electrospinning of poly(glycolic acid) with sucrose particles 436178. International Journal of Polymer Science 2010;2010. https://doi.org/10.1155/2010/436178.

[76] Badmus M, Liu J, Wang N, Radacsi N, Zhao Y. Hierarchically electrospun nanofibers and their applications: A review. Nano Materials Science 2020. https://doi.org/10.1016/j.nanoms.2020.11.003.

[77] Kim JS, Im BG, Jin G, Jang JH. Tubing-Electrospinning: A One-Step Process for Fabricating Fibrous Matrices with Spatial, Chemical, and Mechanical Gradients. ACS Applied Materials and Interfaces 2016;8:22721–31. https://doi.org/10.1021/acsami.6b08086.

[78] Hotaling NA, Bharti K, Kriel H, Simon CG. DiameterJ: A validated open source nanofiber diameter measurement tool. Biomaterials 2015;61:327–38. https://doi.org/10.1016/j.biomaterials.2015.05.015.

[79] Ghafari R, Scaffaro R, Maio A, Gulino EF, lo Re G, Jonoobi M. Processing-structure-property relationships of electrospun PLA-PEO membranes reinforced with enzymatic cellulose nanofibers. Polymer Testing 2020;81:106182. https://doi.org/10.1016/j.polymertesting.2019.106182.

[80] Rwei SP, Huang CC. Electrospinning PVA solution-rheology and morphology analyses. Fibers and Polymers 2012;13:44–50. https://doi.org/10.1007/s12221-012-0044-9.

[81] Naebe M, Lin T, Tian W, Dai L, Wang X. Effects of MWNT nanofillers on structures and properties of PVA electrospun nanofibres.

Nanotechnology 2007;18. https://doi.org/10.1088/0957-4484/18/22/225605.

Figures:

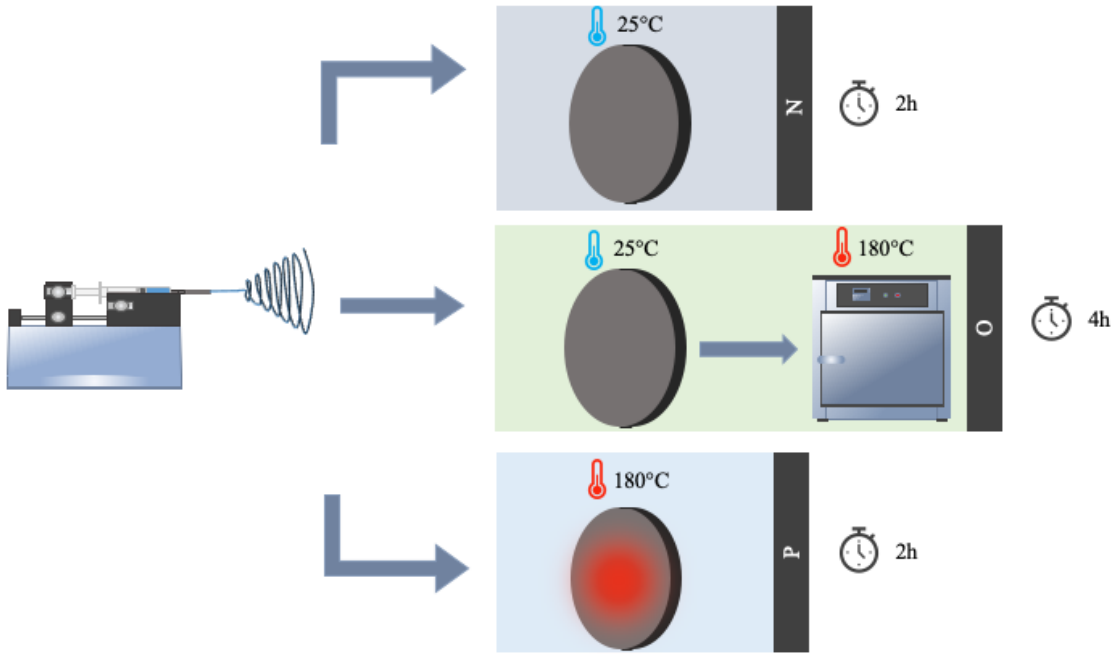

Figure 1. Routes followed for the fabrication of untreated (top) and crosslinked membranes, achieved by post-processing thermal treatment in oven (middle) and in situ heating treatment during electrospinning (bottom).

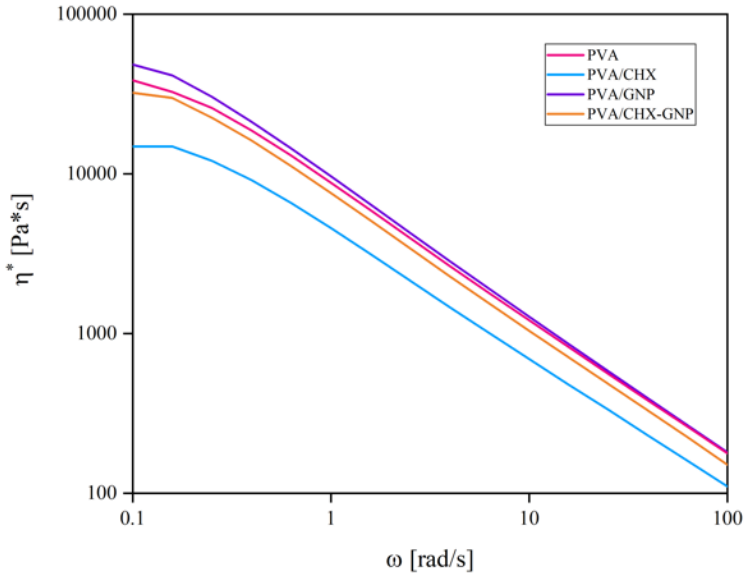

Figure 2. Complex viscosity of the polymeric solutions.

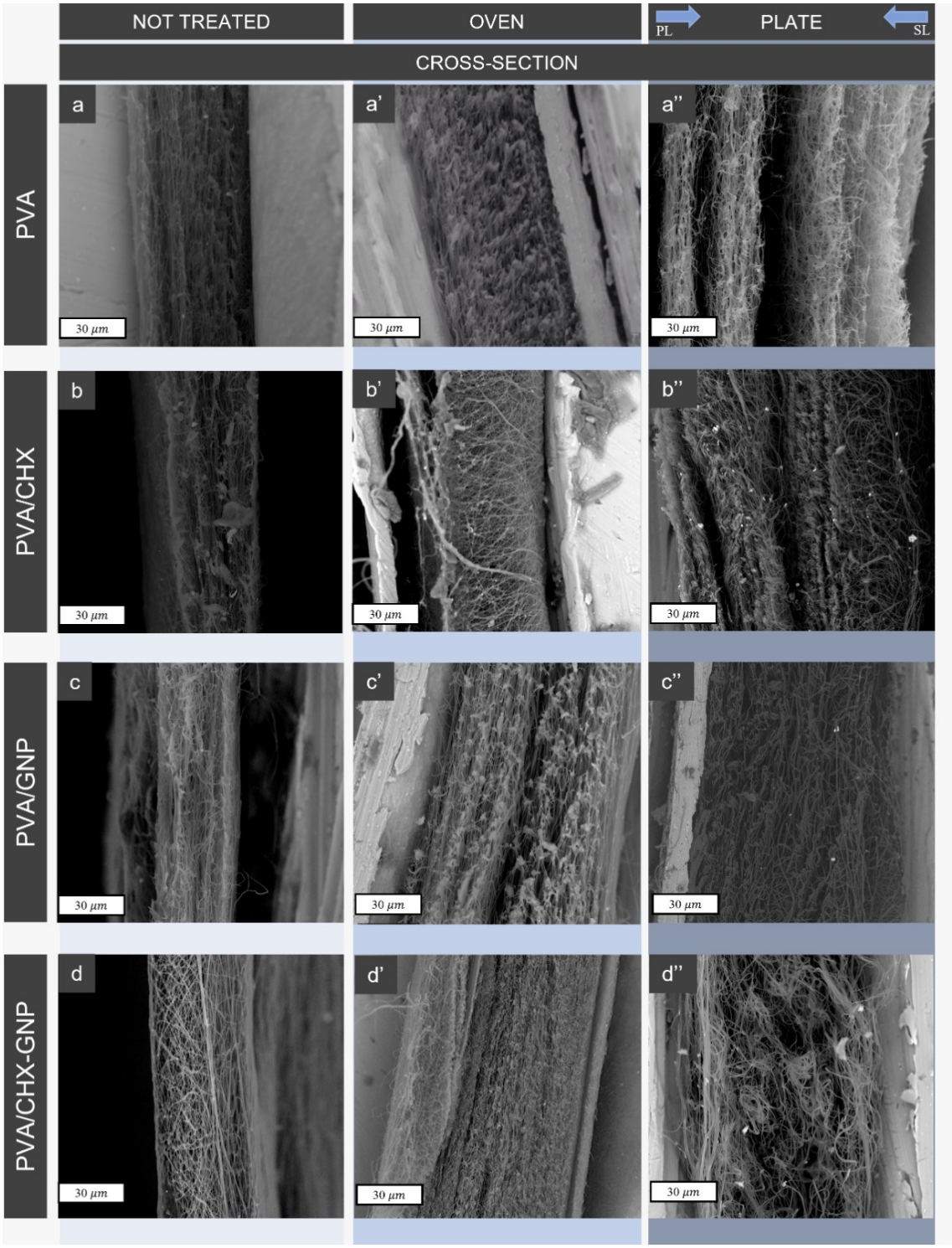

Figure 3. Cross-sectional SEM micrographs of non-treated; oven-treated and plate treated PVA (a, a', a''); PVA/CHX (b, b', b''); PVA/GNP (c, c', c''); PVA/CHX-GNP (d, d', d'').

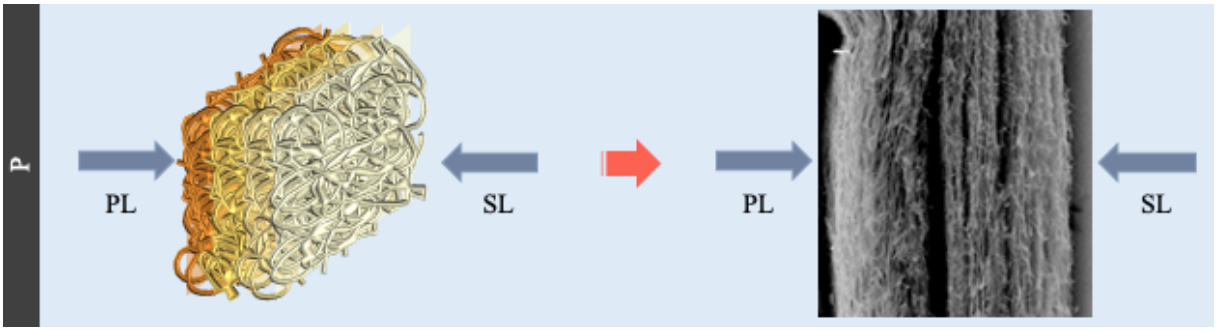

Figure 4. Scheme representing plate crosslinked membrane.

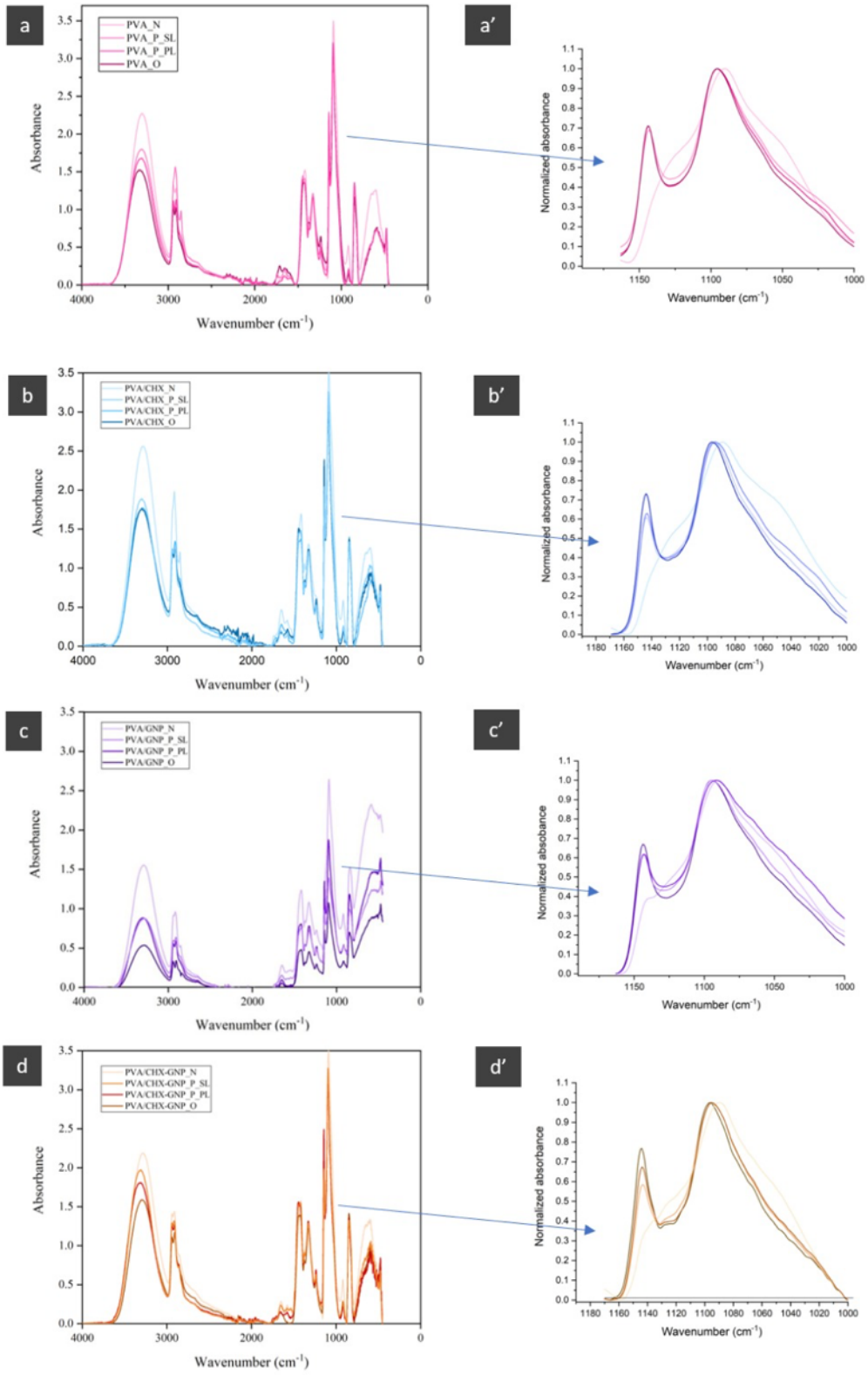

Figure 5. ATR-FTIR spectra of the fibrous membranes, together with close-up of spectral range: 1180-1000 cm-1, normalized to the intensity of peak at 1084/1091 cm-1.

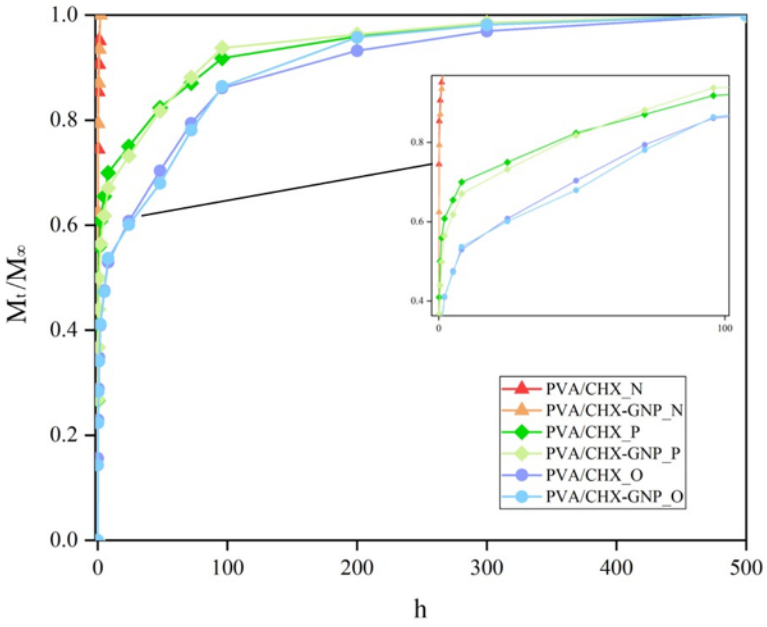

Figure 6. Release kinetics of CHX from membranes in deionized water at 37 °C expressed as m_t/m_∞.

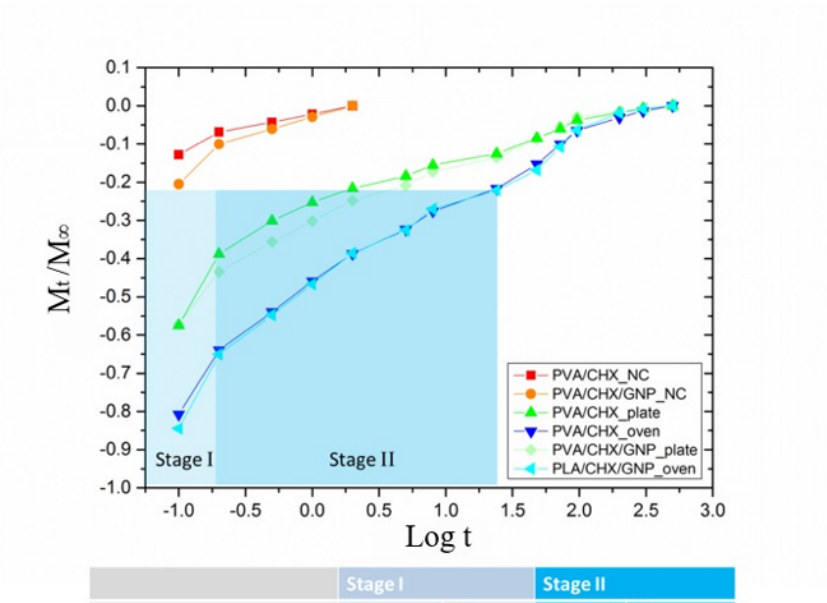

	Stage I		Stage II	
Sample	n	k	n	k
PVA/CHX_plate	0.62	1.111	0.258	0.552
PVA/CHX_oven	0.558	0.562	0.206	0.338
PVA/CHX/GNP_plate	0.456	0.766	0.186	0.498
PVA/CHX/GNP_oven	0.645	0.630	0.265	0.342

Figure 7. Power law model applied to the release data collected in the burst region (m_t/m_∞ <0.6), blue-colored portion of the plot, together with the values of slopes (n) and intercepts (k) of fitting straight lines.

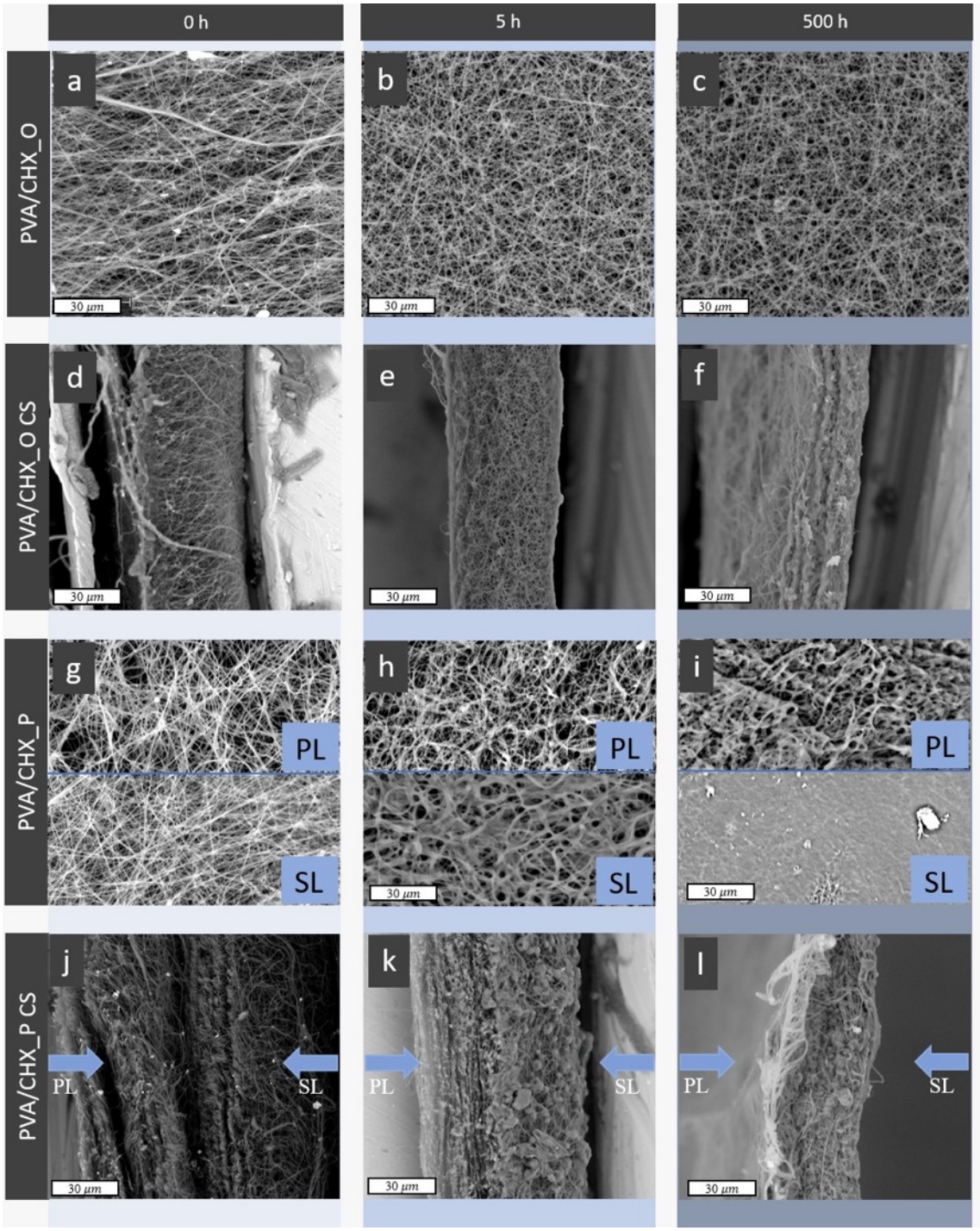

Figure 8. SEM micrographs of section and surface of a-f) PVA/CHX_OVEN and g-l) PVA/CHX_PLATE membrane after soaking in water for 0, 5 and 500h.

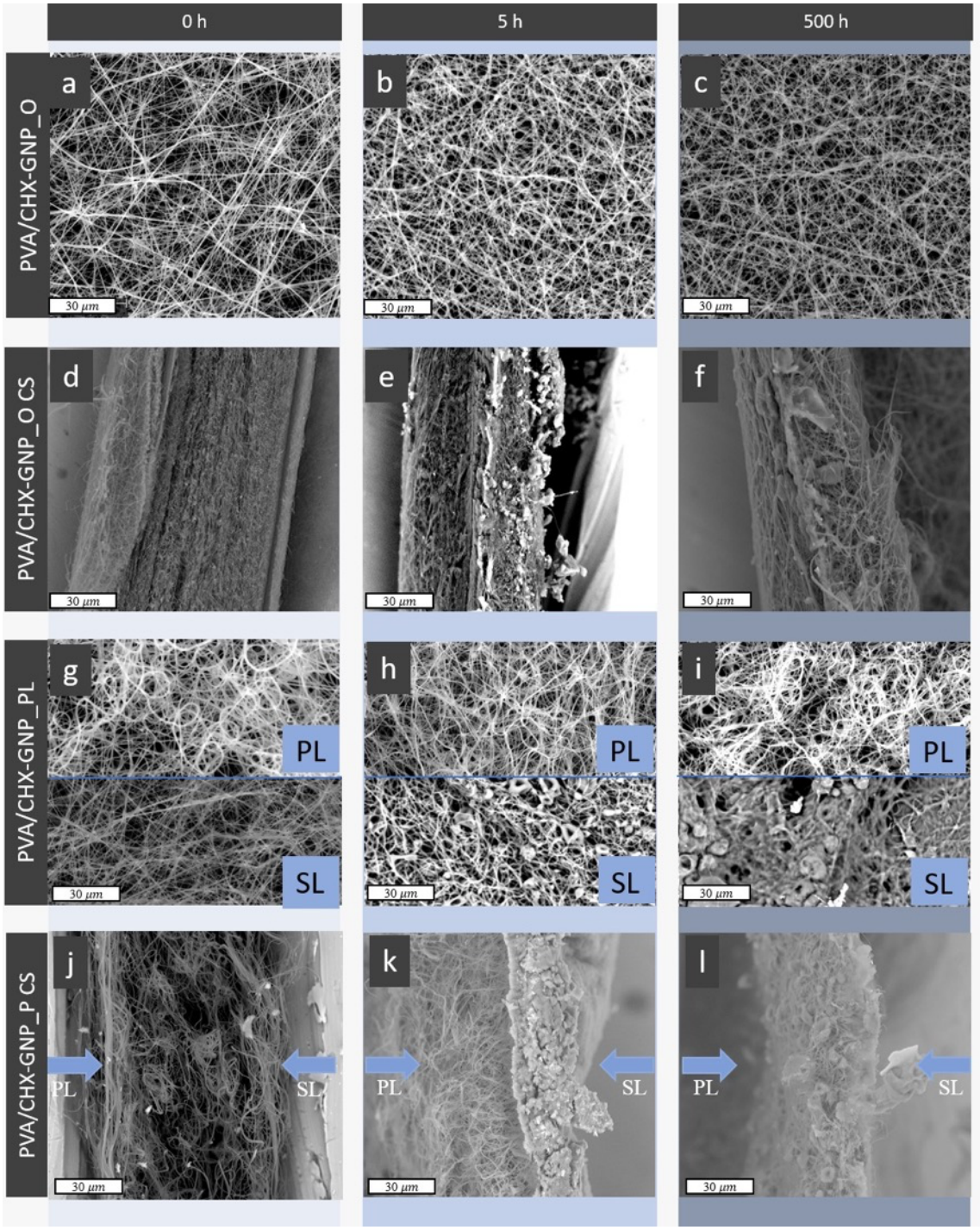

Figure 9. Cross-sectional and surface of a-f) PVA/CHX-GNP_OVEN and g-l) PVA/CHX-GNP_PLATE membrane after soaking in water for 0, 5 and 500h.

Tables:

Table 1. Codename, formulation and preparation route of the systems investigated.

Codename	Formulation			Preparation route	
	PVA (wt.%)	CHX (wt.%)	GNP (wt.%)	Processing	Time (hours)
PVA_N	100	-	-	Electrospinning at 25°C	2
PVA/CHX_ N	98	2	-		
PVA/GNP_ N	99	-	1		
PVA/CHX-GNP_ N	97	2	1		
PVA_ O	100	-	-	Electrospinning at 25 °C plus post-processing treatment in oven at 180 °C	2+2
PVA/CHX_O	98	2	-		
PVA/GNP_O	99	-	1		
PVA/CHX-GNP_O	97	2	1		
PVA_P	100	-	-	In situ thermal treatment (180 °C) during electrospinning	2
PVA/CHX_P	98	2	-		
PVA/GNP_P	99	-	1		
PVA/CHX-GNP_P	97	2	1		

Table 2. Crosslinking degree estimated by calculating insoluble fraction after 5 hours immersion in deionized water at 37 °C.

Sample	Crosslinking degree (%)
PVA_N	0 ± 0
PVA_O	100 ± 0
PVA_P	65 ± 3
PVA/CHX_N	0 ± 0
PVA/CHX_O	100 ± 0
PVA/CHX_P	46 ± 4
PVA/GNP_N	30 ± 2
PVA/GNP_O	100 ± 0
PVA/GNP_P	80 ± 5
PVA/CHX-GNP_N	25 ± 2
PVA/CHX-GNP_O	100 ± 0
PVA/CHX-GNP_P	68 ± 3

Table 3. Elastic modulus (E), tensile strength (TS), and elongation at break (EB) of the electrospun membranes.

Sample	E (MPa)	TS (MPa)	EB (%)
PVA_N	84 ± 1.2	5.17 ± 1.6	102 ± 4.4
PVA_O	140 ± 1.9	6.03 ± 0.7	43 ± 3.6
PVA_P	65 ± 1.2	5.05 ± 1.2	64 ± 8.5
PVA/CHX_N	78 ± 4.4	3.36 ± 0.9	153 ± 15.2
PVA/CHX_O	114 ± 1.9	5.67 ± 1.6	53 ± 7.2
PVA/CHX_P	57 ± 1.3	3.04 ± 1.5	64 ± 2.1
PVA/GNP_N	150 ± 6.1	5.17 ± 0.1	41 ± 1.7
PVA/GNP_O	170 ± 2.9	2.31 ± 0.2	29 ± 5.7
PVA/GNP_P	151 ± 3.7	3.77 ± 0.6	56 ± 6.9
PVA/CHX-GNP_N	142 ± 1.5	2.76 ± 0.4	58 ± 1.6
PVA/CHX-GNP_O	160 ± 1.9	2.03 ± 0.1	24 ± 4.3
PVA/CHX-GNP_P	138 ± 0.2	2.64 ± 0.4	45 ± 0.4